Journal of Medicinal Chemistry

Article

pubs.acs.org/jmc

A Frozen Analogue Approach to Aminopyridinylimidazoles Leading to Novel and Promising p38 MAP Kinase Inhibitors

Roland Selig,[†] Marcia Goettert,[†] Verena Schattel,[†] Dieter Schollmeyer,[‡] Wolfgang Albrecht,[§] and Stefan Laufer*,[†]

[†]Department of Medicinal Chemistry, University of Tuebingen, Auf der Morgenstelle 8, 72076 Tuebingen, Germany

[‡]Department of Organic Chemistry, University of Mainz, Duesbergweg 10-14, 55099 Mainz, Germany

[§]c-a-i-r biosciences GmbH, Paul-Ehrlich-Strasse 15, 72076 Tuebingen, Germany

Supporting Information

ABSTRACT: In this study we report the design, synthesis, and biological evaluation of constrained aminopyridinylimidazoles as p38α MAP kinase inhibitors. The frozen analogue approach focused on the pyridinyl unit, using purine bioisosteres as constrained structure analogues. The identification of the most potent bioisostere was followed by a further derivatization to address hydrophobic region II. In combination with C-2 modifications of the imidazole core, we were able to design highly active inhibitors on the p38α MAP kinase. The inhibitor design presented herein represents a promising and highly efficient advancement of recent stages of development in this class of p38 MAP kinase inhibitors. In combination with the highly flexible synthetic strategy, directions toward further investigations of complex C-5 modifications of diarylimidazoles are indicated.

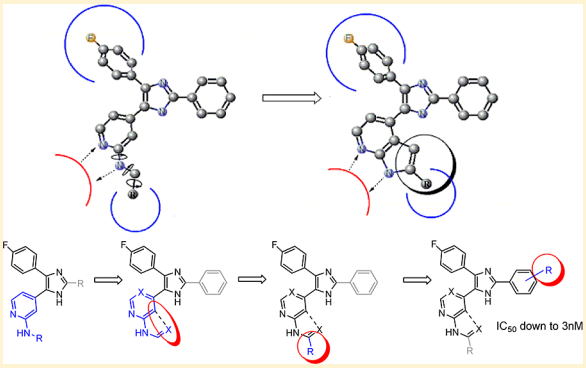

INTRODUCTION

The inhibition of interleukin 1β (IL-1β) production by the anti-inflammatory compound SKF86002[1] (Figure 1) was first reported in 1988,[1] but it was not until 1994 that the molecular target of this class of pyridinylimidazole compounds was identified as p38α mitogen activated protein kinase (MAPK), a serine/threonine kinase. Because of the central role of p38 MAPK in inflammatory bowel disease and rheumatoid arthritis, the inhibition of p38 MAPK became a promising therapeutic strategy. The further development of p38 MAPK inhibitors focused on derivatizations of the core structure of SKF86002, leading to the early lead compound SB203580[2] (Figure 1) with an additional interaction site, the C-2 aryl moiety forming a $\pi-\pi$ stacking to Tyr35.[3] The development of this kind of p38 MAP kinase inhibitors followed a straightforward inhibitor design. The vicinal pyridine 4-fluorophenyl system within this pharmacophore proved to be one of the most efficient and selective systems for binding to p38 MAP kinase, and this structure has been maintained in many p38 inhibitors modeled on SB 203580.[4]

The pyridine nitrogen accepts a hydrogen bond from the backbone of Met109, and the fluorophenyl moiety confers selectivity for MAPK over other PKs because of its interaction with hydrophobic region I (Figure 1).[5]

Further derivatizations were focused on the N1-substituted imidazoles, mainly to reduce interactions with CYP450 enzymes.[4] Boehm and Gallagher reported the detrimental effect of N-substitutions on inhibitor potency, showing that N-substituted pyridinylimidazoles bind to p38 MAP kinase with a generally lower affinity than their N-unsubstituted counterparts.[4,6−8] In a further refinement, alkylated or arylated amines were introduced at the C-2 position of the pyridine moiety, a modification that improved potency and selectivity by formation of an additional hydrogen bond to the hinge region and addressing hydrophobic region II (Figure 1).[9] This kind of modification in combination with the C-2 modifications of the imidazole core lead to highly selective and potent inhibitors with IC_{50} values in the low nanomolar range.

The binding of the ligand to the receptor results in an energy penalty due to the loss of conformational energy that is detrimental to the strength of the binding. Conformational restriction is a commonly used principle to avoid these adverse effects. Reduction in conformational flexibility can be realized by steric hindrance or restriction, which minimizes the entropy−enthalpy compensation by minimizing the loss of conformational entropy[11,12] and therefore enhance potency as well as selectivity of the corresponding ligands. As investigated by Veber et al., the characteristics of the ligands are markedly improved by freezing rotatable bonds. In this study a correlation between the bioavailability of a compound and the number of rotatable bonds was shown, irrespective of the

Received: June 17, 2012
Published: September 6, 2012

dx.doi.org/10.1021/jm300852w | J. Med. Chem. 2012, 55, 8429−8439

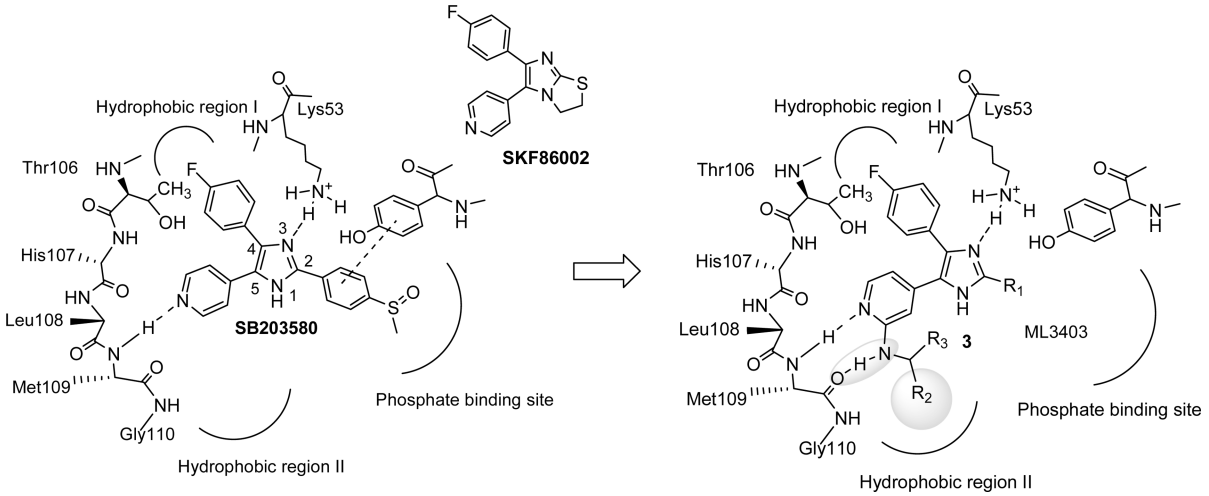

Figure 1. Structures of pyridinyl imidazole compound SKF86002 and derivatives SB203580 (left) and ML3403 (right), showing binding mode of SB203580 and sites of derivatization of SB203580 (R_1= various residues, aryl, SMe, H, alkinyl; R_2= hydrophobic residues; R_3 = H, alkyl) and ML3403[10] (R_1 = SMe; R_2 = phenyl; R_3 = Me).

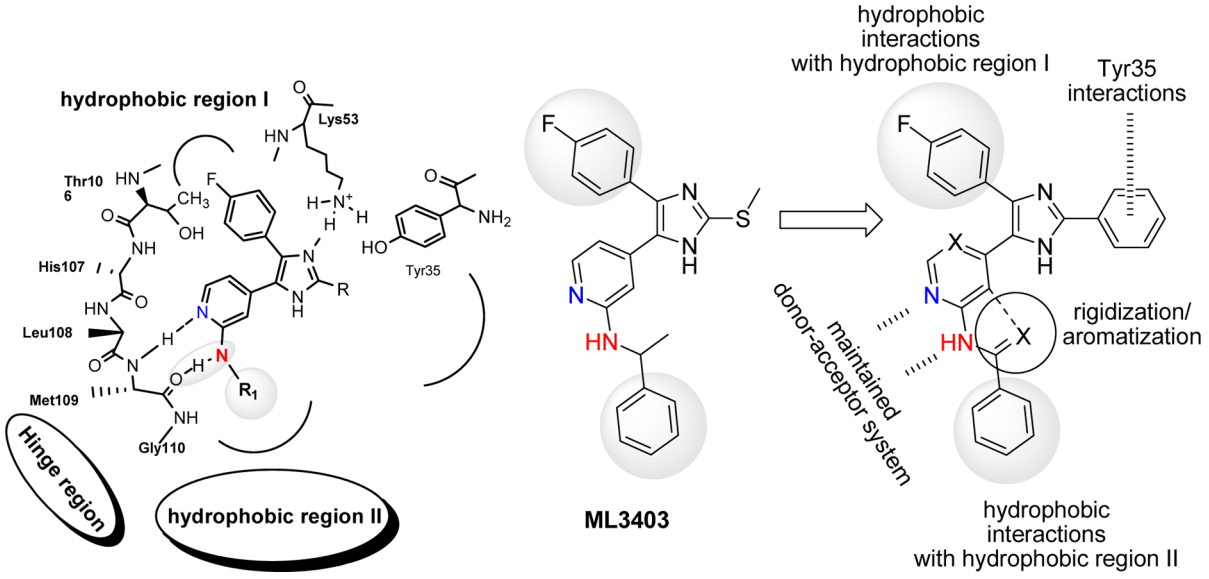

Figure 2. Rigidization concept based on ML3403.

molecular weight. The resulting findings of this study showed that even the Lipinsky rule in regard to the molecular weight might be circumvented using a frozen analogue approach.[13]

Taken in this context, we proposed to further develop the class of aminopyridinylimidazoles using a rigidization strategy and to focus on the most effective protein−ligand interaction site, the C-5 scaffold. A highly effective, literature-known aminopyridine residue proved to be the methylphenylamine moiety of ML3403 (Figure 1), which served as a starting point for our investigations. Maintaining the highly effective donor−acceptor system of the aminopyridinyl system, we investigated purine bioisosteres as new C-5 rigidized aminopyridinyl scaffolds of the imidazole core with implemented aromatization (Figure 2). Among the various C-2 modifications at the imidazole core, we chose, in contrast to ML3403, phenylation of the C-2 residue in order to maintain the $\pi-\pi$ stacking interaction with Tyr35.

CHEMISTRY

We followed a straightforward synthetic procedure involving a convergent strategy (Scheme 1) that was based on C−C cross-coupling reactions, as recently published by our group.[14] This high yielding synthesis was optimized by ligand screening and technical modifications with regard to mechanistic details.

The challenge of this cross-coupling reaction was to combine activated (purine and pyrrolopyrimidine) and deactivated substrates (azaindoles) as cross-coupling partners in a single robust process. The deactivated chlorinated azaindoles were especially sensitive to the destannylation process as the dominant side reaction, lowering the yields and reaction rates dramatically. In our investigations of the detrimental side reactions and reaction rates, changing the ligand sphere from the initially used PPh_3 to X-Phos proved to be the most effective modification. The high efficiency of the X-Phos ligand system is proposed to arise from the monocoordinated Pd species[15] that facilitates both the oxidative addition and the transmetalation step. The mechanism of the Stille coupling with

dx.doi.org/10.1021/jm300852w | J. Med. Chem. 2012, 55, 8429−8439

Scheme 1. Synthesis of the Tested Compounds[a]

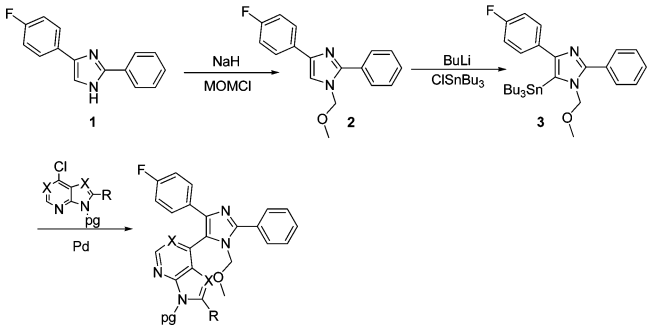

[a]X = CH, N; pg = protecting group; R = H, cyclohexyl, phenyl, benzyl, annelated phenyl.

PPh_3 was substrate specific with the electron poor heterocycles 6-chloro-9-(tetrahydro-2*H*-pyran-2-yl)-9*H*-purine[16] (**4**) and 4-chloro-7-(methoxymethyl)-7*H*-pyrrolo[2,3-*d*]pyrimidine[14] (**5**), following the established rate determining step, the transmetalation. In contrast, the rate determining step of the Stille coupling with 4-chloro-1-(phenylsulfonyl)-1*H*-pyrrolo[2,3-*b*]-pyridine[17] **6** was determined to be the oxidative addition (Scheme 2), when using PPh_3 as the ligand system.[14]

Scheme 2. Effect of the Substrate on the Stille Cross-Coupling and the Rate Determining Steps

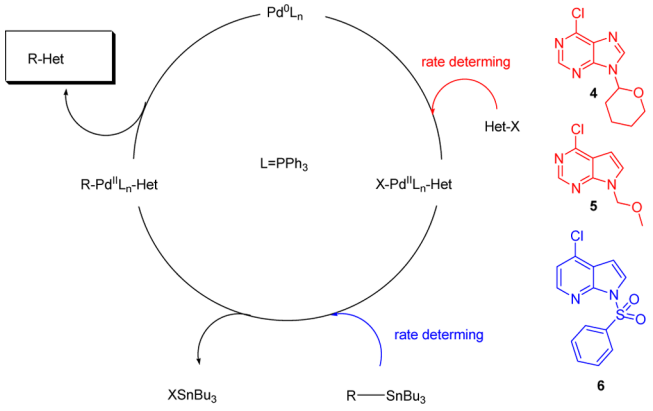

In the present study, we have extended our chemical investigations of this synthetic procedure, based on a solvent screening approach with the intention of further optimization of the existing synthetic procedure.

First, we endeavored to clarify the question of the rate determining step in the Stille cross-coupling when using 2-dicyclohexylphosphino-2′,4′,6′-triisopropylbiphenyl (X-Phos) as the ligand system and **6** as the substrate for oxidative addition (Scheme 2). A change in the mechanism with X-Phos is likely. In our published study we showed that the oxidative addition was the rate determining step in the case of triphenylphosphine (PPh_3) as the ligand system. With X-Phos, we presumed that the transmetalation had become the rate determining step. Our measurements of the time-dependent turnover numbers (Scheme 3) revealed a clear dependency on the concentration of the stannylated compound **3** (Figure 3). The direct dependence on the stannyl concentration indicated that the transmetalation was the rate determining step. This inversion of the rate determining step to favor the transmetalation reaction with **6** indicated that the

Scheme 3. Representative Cross-Coupling Reaction of 6 and 4-(4-Fluorophenyl)-1-(methoxymethyl)-2-phenyl-5-(tributylstannyl)-1*H*-imidazole[18] (7) in 2 mL of DMF at 83 °C under Argon Atmosphere

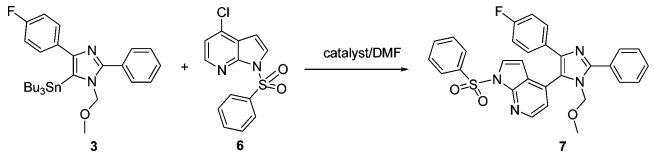

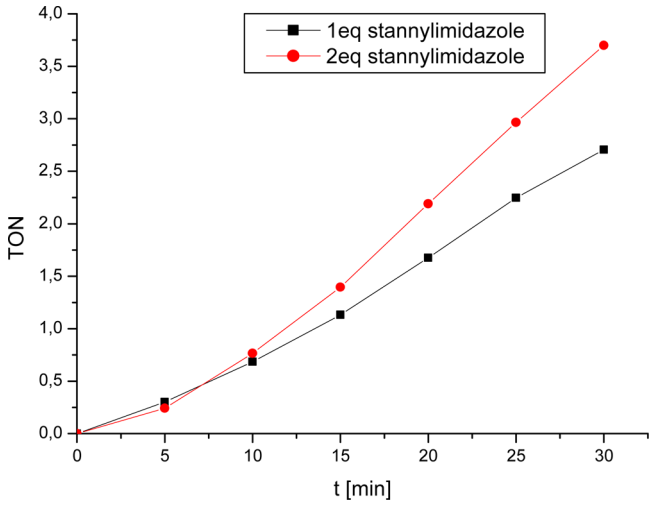

Figure 3. Effect of the concentration of the stannylimidazole on the turnover numbers (TON) in the cross-coupling reaction as a function of time at 83 °C in 3 mL of DMF, quantified by HPLC.

chlorinated substrates would be more advantageous than the bromo or iodo species for the cross-coupling process. The cross-coupling reaction to obtain **7** was performed with **6** and the corresponding stannylimidazole **3** (Scheme 3).

Since the mechanistic course of the cross-coupling reaction is influenced by the nature of the ligands, factors that stabilize the essential intermediates of the Pd species ought to further increase the reaction rates. We therefore examined the stabilizing effects of the solvents.

For an optimization of the cross-coupling reaction with PPh_3, an accelerating effect of the solvent would be expected to assist the rate determining oxidative addition.

The rate determining step with X-Phos was shown to be the transmetalation. Coordinating solvents should also play a beneficial role in this step because of their capability of stabilizing the three coordinated intermediates. The solvents used in our study ranged from weakly coordinating to strongly coordinating solvents, ranked as follows: toluene, THF, dioxane, DMSO, NMP, DMF.

Using quantitative HPLC, we investigated the effects of the solvent on the turnover frequencies of the two different catalyst systems at 76 °C (Figure 4). As representative substrates for the cross-coupling reaction, we chose the chlorinated phenylsulfonyl protected 7-azaindole **6** and the stannylated diarylimidazole **7** as substrates (Figure 4). Toluene and dioxane were the most effective solvents in the cross-coupling reaction with $PdCl_2(PPh_3)_2$ as precatalyst. DMSO showed a moderate turnover frequency, while the reaction rates with DMF and NMP were very low (Figure 4).

Weakly coordinating and moderately coordinating solvents were favored, which is in contrast to the expected results. The

dx.doi.org/10.1021/jm300852w | J. Med. Chem. 2012, 55, 8429−8439

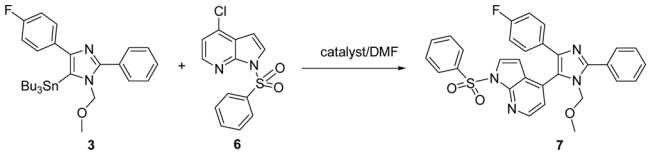

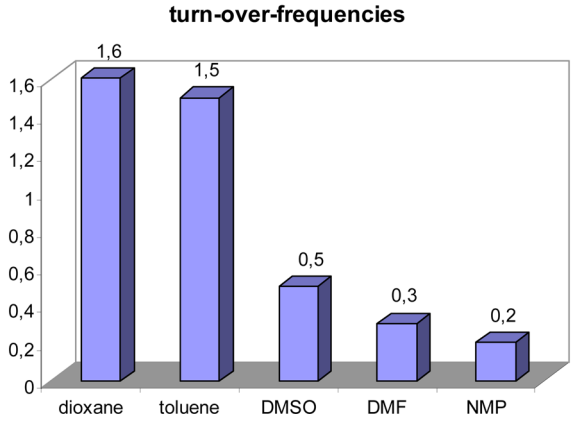

Figure 4. Effect of the solvent on the turnover frequencies in the cross-coupling reaction performed at 76 °C with $PdCl_2(PPh_3)_2$ as precatalyst (Table 1, entries 1–5).

Table 1. Optimization of the Cross-Coupling Reaction: Comparison of the Effects of Pd Ligand, Solvent, Reaction Temperature, and Reaction Time

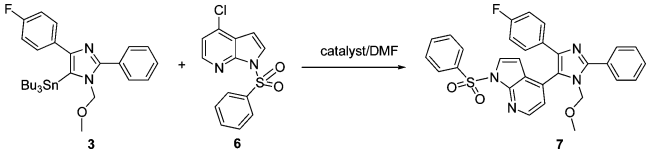

entry	catalyst	conditions[a]	t [min]	yield [%][b]
1	$PdCl_2(PPh_3)_2$, 17 mol %	DMF/76 °C	30	3
2	$PdCl_2(PPh_3)_2$, 16 mol %	NMP/76 °C	30	2
3	$PdCl_2(PPh_3)_2$, 18 mol %	DMSO/76 °C	30	4
4	$PdCl_2(PPh_3)_2$, 14 mol %	toluene/76 °C	30	10
5	$PdCl_2(PPh_3)_2$, 16 mol %	dioxane/76 °C	30	13
6	$Pd(OAc)_2$/X-Phos, 10 mol %	DMF/76 °C	30	93
7	$Pd(OAc)_2$/X-Phos, 10 mol %	NMP/76 °C	30	78
8	$Pd(OAc)_2$/X-Phos, 10 mol %	DMSO/76 °C	30	8
9	$Pd(OAc)_2$/X-Phos 10 mol %	toluene/76 °C	30	47
10	$Pd(OAc)_2$/X-Phos, 10 mol %	dioxane/76 °C	30	22
11	$Pd(OAc)_2$/X-Phos, 12 mol %	DMF/76 °C	10	15
12	$Pd(OAc)_2$/X-Phos, 11 mol %	DMF/95 °C	30	51
13	$Pd(OAc)_2$/X-Phos, 10 mol %	DMF/102 °C	30	92
14	$Pd(OAc)_2$/X-Phos, 12 mol %	DMF/76 °C	20	24
15	$Pd(OAc)_2$/X-Phos, 12 mol %	DMF/76 °C	67	2

[a]Conditions: 1 equiv of **6**, 2 equiv of **3** in 3 mL of solvent for indicated reaction time. [b]Quantified by HPLC.

strong coordination of DMF leading to the PPh_3-Pd-DMF/$[DMF\text{-}Pd\text{-}Cl]^-$ species, as assumed by Ahlquist et al.,[19] may have prevented effective coordination of Pd to the weakly electrophilic center of **6**. The reduced coordination capacity of toluene and dioxane seems to be crucial in forming the oxidative addition complex in the case of the deactivated halogen substrates, such as **6**, possibly because of the lower substrate–Pd affinity which is further reduced by the competing solvent–Pd coordination.

Further investigations focused on the highly efficient X-Phos ligand system (Figure 5). The solvent screening of this system was analogous to that of PPh_3.

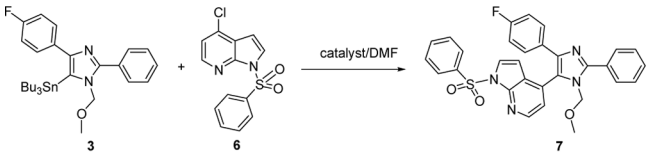

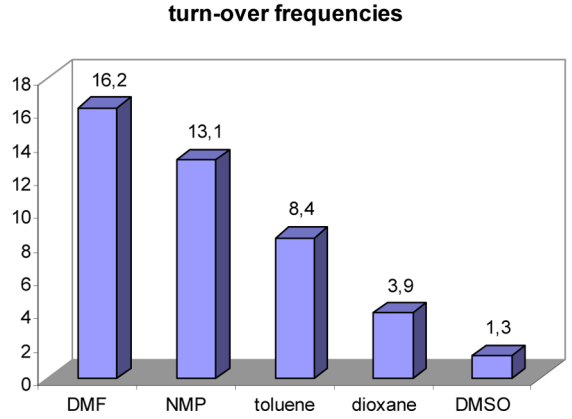

Figure 5. Effect of the solvent on the turnover frequencies in the cross-coupling reaction performed at 76 °C with a premilled mixture of $Pd(OAc)_2$ and X-Phos (1/3) as precatalyst (Table 1, entries 6–10).

A different reactivity profile was obtained with X-Phos that was at odds with the predicted order of the solvent coordination capacity. Moderately coordinating solvents were disfavored in the transmetalation step with X-Phos as ligand sphere. In contrast to PPh_3 (Figure 4), strongly coordinated DMF proved to be the most effective solvent with X-Phos (Figure 5).

Compared to dioxane, NMP and toluene also strongly accelerated the reaction rates, whereas DMSO afforded lower turnover frequencies. Coordinating solvents showed a positive influence. The most attractive solvent in our recently published study was dioxane, which proved to be also the most efficient solvent with PPh_3 in the present study. However, using dioxane with the more efficient X-Phos ligand system was disadvantageous, giving a 4-fold slower reaction rate than DMF (Figure 5).

To further investigate the accelerating solvent effect of DMF with X-Phos, we examined the effect of temperature on the turnover frequencies (Figure 6). The optimum turnover frequency was obtained at 102 °C and was in the range of our earlier study with microwave irradiation.[14] Thus, conventional heating with DMF as solvent led to highly efficient conversions at low temperatures.

In conclusion, the cross-coupling procedure was further optimized by solvent assisting effects. The high reaction rates showed the efficiency of the catalytic system even at 102 °C, without the need for microwave irradiation. The change of the

dx.doi.org/10.1021/jm300852w | J. Med. Chem. 2012, 55, 8429–8439

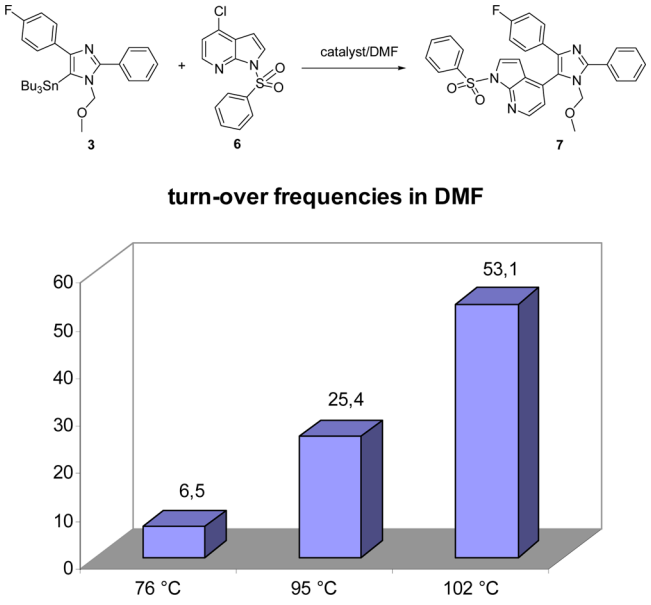

Figure 6. Effect of temperature on the turnover frequencies in the cross-coupling reaction in the presence of X-Phos as Pd ligand (Table 1, entries 11−13).

solvent from dioxane to DMF allowed an expanded temperature range with the option of even higher reaction rates. With these reaction rates, the catalyst loadings can be significantly reduced to low levels.

The choice of the protecting groups was applied to the final target compounds (Scheme 4). The investigation of N-

Scheme 4. Preparation of 10 and 12: Deprotection Procedures

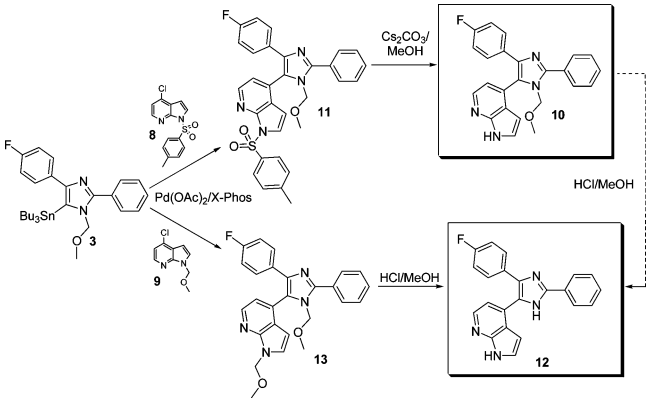

substitution led us to select an orthogonal strategy with 4-chloro-1-tosyl-1*H*-pyrrolo[2,3-*b*]pyridine[20] (**8**) and the methoxymethyl (MOM) protected imidazole core. The detosylation was accomplished with Cs_2CO_3[21,22] in refluxing methanol, leading to the MOM protected target compound 4-(4-(4-fluorophenyl)-1-(methoxymethyl)-2-phenyl-1*H*-imidazol-5-yl)-1*H*-pyrrolo[2,3-*b*]pyridine (**10**) (Scheme 4).

In this study the most potent structures in regard to their biological activities were shown to be the N-unsubstituted analogues of **12**. For their synthesis we chose a parallel deprotection procedure with methoxmethyl as the dual protecting group in compound **13**.[6] The deprotection procedure followed established methods, using concentrated HCl_{aq} in refluxing MeOH (Scheme 4) to remove both MOM groups.[23]

BIOLOGICAL EVALUATIONS

On the basis of our concept to investigate purine bioisosteres as new rigidized C-5 scaffolds of the aminopyridinyl moieties, we developed a strategy based on five stages (Figure 7). Stage I

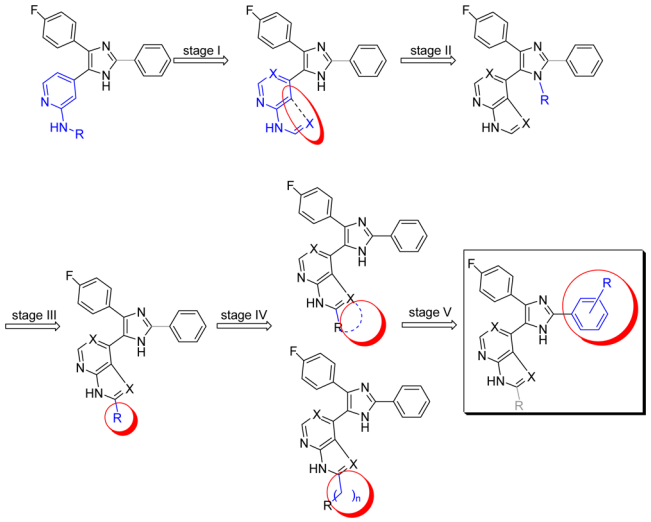

Figure 7. Strategic concept for investigation of purine bioisosteres.

investigations focused on the identification of the most potent purine bioisostere. In stage II, we investigated the influence of N-substituents on the imidazole core. The objective of stage III was to address the hydrophobic region II of MAPK by further lipophilic modifications of the most effective purine bioisostere in the inhibitors. The investigations of stage IV examined the impact of further enhancing or diminishing the rigidization of the substituted purine scaffold. The final stage V involved improving the potency of the evaluated inhibitor with literature-known modifications of the 2-phenyl residue at the imidazole core.

Our incipient effort at inhibitor design at stage I was to develop a potent isosteric scaffold of the aminopyridinyl moiety. The 7-azaindole is the most obvious rigidized structural analogue of the aminopyridinyl unit, but we also examined a series of bioisosteres with purine and pyrrolopyrimidine substituents as potential candidates (**14a** and **14b**) (Figure 8).

To directly compare biological activity, we chose a fixed core structure; in the case of C-5 derivatizations, we examined the C-2 phenylation of 4-(4-fluorophenyl)-2-phenylimidazole (Figure 8, structure **14**/**15**).

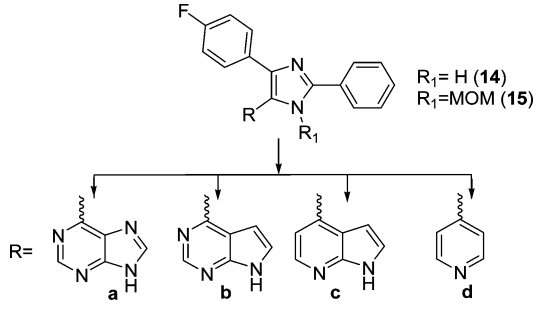

Figure 8. C-5 modifications of the imidazole core.

dx.doi.org/10.1021/jm300852w | J. Med. Chem. 2012, 55, 8429−8439

With IC_{50} values of 740 nM (**14a**), 2600 nM (**14b**), and 108 nM (**14c**), the 7-azaindole substituent was identified as the most potent C-5 scaffold (Table 2 and Figure 10). Compared

Table 2. Inhibition of p38 MAPK

compd	IC_{50} [μM][a]	activity coefficient, IC_{50}(SB203580)/IC_{50}(compd)
14a	0.740 ± 0.1169	0.10
14b	2.600 ± 0.0862	0.03
14c	0.108 ± 0.0012	0.47
14d	0.154 ± 0.0092	0.33
15a	2.989 ± 0.0582	0.01
15c	0.451 ± 0.0589	0.18

[a]Mean ± SEM of three experiments. Compounds tested according to Laufer et al.[24]

to the reference compound 4-(4-(4-fluorophenyl)-2-phenyl-1*H*-imidazol-5-yl)pyridine (**14d**), a 1.4-fold increase in potency with an activity coefficient of 0.47 (IC_{50}(SB203580 (**2**))/IC_{50}(compound)) was assigned to **14c**.

Maintaining the most potent C-5 scaffold, the 7-azaindole, we investigated in stage II the impact of the N1-derivatizations, widely used optimization sites in literature compounds and mainly used to reduce CYP450 interactions.[7] We assumed a negative effect of these derivatizations, due to disadvantageous conformational effects of the azaindole moiety, which is flipping out of the biological relevant conformation by the repulsion of the N-residues (Figure 9). The flexibility of the known

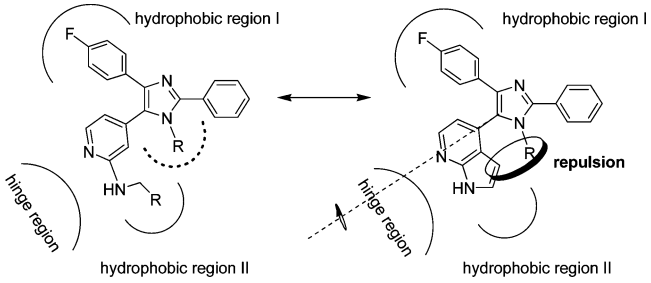

Figure 9. Conformational effects of N1 substituents.

aminopyridinylimidazoles provides a better conformational tolerance, due to the possible independent torsion opportunities of the free rotatable C−N−C bonds. This rigidization, leading to the 7-azaindole, results in the repulsion of the entire C-5 moiety, effectively disturbing the hinge region interaction.

The decreased conformational tolerance of the new rigidized structure analogues is reflected in their loss of biological activities, with a 10- and nearly 3-fold decrease in potency, respectively, of compounds **15a** and **15c** compared to their unsubstituted analogues **14a** and **14c** (Table 2).

In stage III, the further development of the 7-azaindole moiety focused on addressing interactions with the hydrophobic region II (Figure 10). Among the wide range of accomplished modifications in recent years, phenyl substituents such as phenylethylamine[9] have been among the most promising residues addressing this region. Therefore, we expanded the azaindole scaffold to include the 2-phenylated system, the rigidized analogue to the aminopyridine moiety of ML3403 (Figure 2). With an IC_{50} of 16 nM (Table 3) the compound **14f** showed a 7-fold improved activity profile with

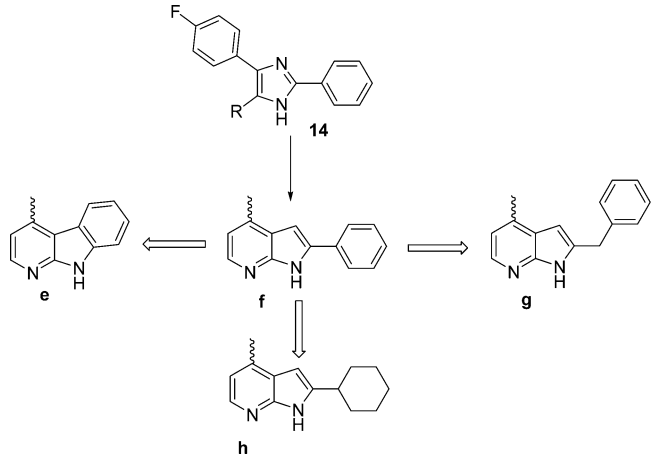

Figure 10. Lipophilic substitution of 7-azaindole to address the hydrophobic region II.

respect to the reference compound **14d** (Table 2) (compared by activity coefficients).

Table 3. Inhibition of p38 MAPK by Substituents That Affect the Interactions with Hydrophobic Region II

compd	IC_{50} [μM][a]	activity coefficient, IC_{50}(SB203580)/IC_{50}(compd)
14e	0.153 ± 0.0398	0.55
14f	0.016 ± 0.0038	2.38
14g	0.345 ± 0.0319	0.07
14h	0.015 ± 0.0003	2.07

[a]Mean ± SEM of three experiments. Compounds tested according to Laufer et al.[24]

To enhance the entropic effect, we dearomatized the phenyl moiety to the more bulky cyclohexyl analogue **14h** (Figure 10) in order to expand the lipophilic surface. Nevertheless, the phenyl residue of **14f** (Figure 10) proved to be the more efficient residue to address the hydophobic region II with an activity coefficient of 2.38, whereas the activity coefficient of **14h** was shown to be slightly lowered with 2.07 (Table 3).

The strategy of stage IV was to examine the impact of rigidization on the 2-phenylated azaindole scaffold. With α-carboline the maximum rigidized structure analogue (**14e**) (Figure 10) to address hydrophobic region II was synthesized.

With an IC_{50} of 153 nM and an activity coefficient of 0.55 the carboline **14e** showed only a slightly increased activity profile (Table 3) compared to the unsubstituted azaindole derivative **14c** (Table 2), despite the extended possible hydrophobic interaction side provided by the annelated phenyl residue.

Two disadvantageous synergistic effects were assumed to be responsible: the lack of flexibility and the steric demand of the carboline. Because of the annelated phenyl moiety, the steric demand of the azaindole is negatively expanded in the direction to the imidazole core, resulting in a putative increased energy penalty to the biologically relevant conformation. Docking studies carried out to evaluate these assumptions confirmed a disturbed $\pi-\pi$ stacking with Tyr35 (Figure 11), due to the steric repulsion of the carboline plane from the imidazole plane, with the consequence of increased interaction distances. The obvious lack of flexibility of the phenyl moiety with respect to the hydrophobic interaction with the hydrophobic region II is a further detrimental effect of this rigidization. The loss of the

dx.doi.org/10.1021/jm300852w | J. Med. Chem. 2012, 55, 8429−8439

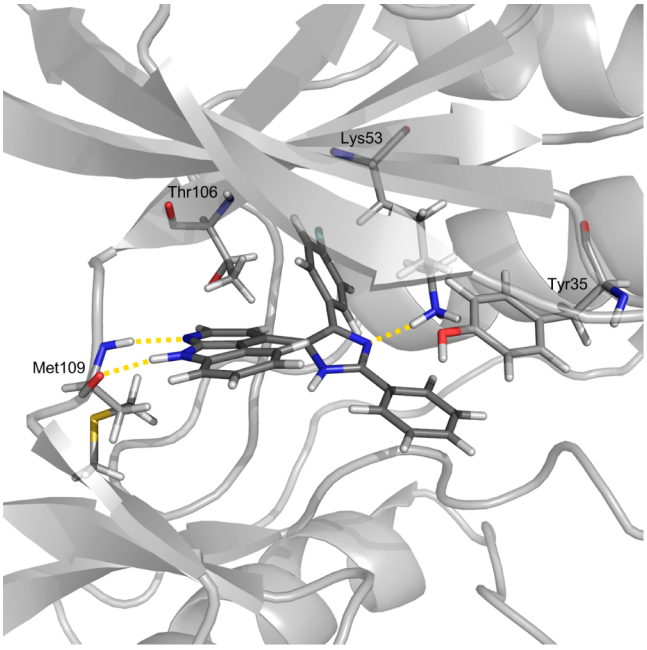

Figure 11. Docking results for **14e** in the p38 MAP kinase. X-ray structure 1YWR[20] is from the PDB database.

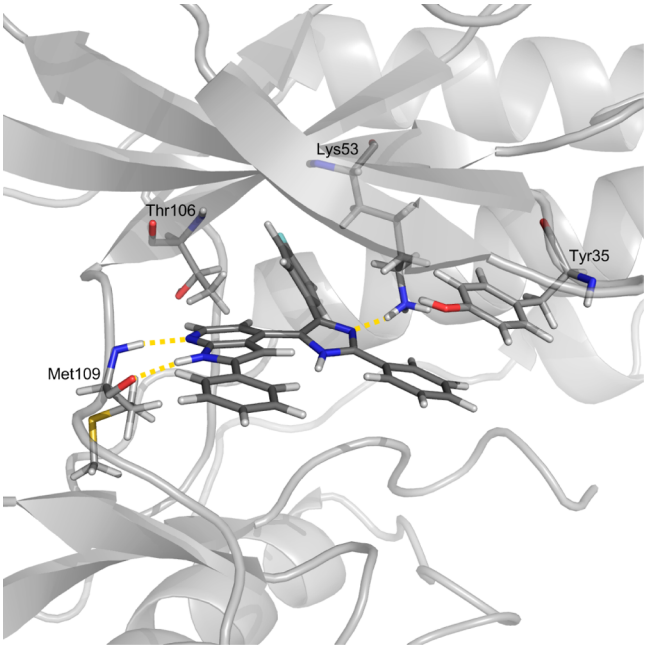

Figure 12. Docking results for **14f** in the p38 MAP kinase. X-ray structure 1YWR[25] is from the PDB database.

C−N−C torsion possibilities and the predetermined prejudicial orientation of the annelated phenyl residue lead to a reduced capability for ideal interactions with hydrophobic region II.

The disadvantageous elements of the carboline scaffold may be avoided by using the aforementioned 2-phenyl substituted azaindole derivative **14f** (Figure 10). The essential flexibility is given, and a possible repulsion with the imidazole core is circumvented by the sterically neutral orientation of the phenyl substituent.

Docking experiments with **14f** indicated advantageous torsion angles for the diarylimidazole and the azaindole plane for interactions with Tyr35 (Figure 12). The C-2 (azaindole) phenyl moiety and the azaindole are slightly twisted in relation to one another, and the orientation of the phenyl residue, addressing hydrophobic region II, is markedly different from that of the carboline substituted derivative **14e** (Figures 11 and 12), leading to an improved hydrophobic interaction.

A further loss of rigidization by the benzylated azaindole **14g** (Figure 10) led to a dramatic decrease in potency with an IC_{50} of 345 nM (Table 3).

With the accomplishment of these derivatizations, the lead structure of the C-5 scaffold was identified as the 2-phenylazaindole **14f**.

The nonrigidized counterpart ML3403 (Figure 2) of the 2-phenylazaindole scaffold, the phenylmethylamine substituted pyridine, proved to be a highly potent derivative, with the assumption that the hydrophobic interaction sites were extended, as provided by the hydrophobic interaction sites above and below the pyridine ring.[9] This beneficial effect was reduced by our rigidization concept because of the integration of the methyl residue into the rigidized aromatic system.

The 1YWR crystal was chosen for docking experiments. The ligand ((*S*)-4-(4-fluorophenyl)-1-methyl-5-(2-(1-phenylethylamino)pyrimidin-4-yl)-2-(piperidin-4-yl)-1,2-dihydropyrazol-3-one) bound in X-ray structure 1YWR shows that the benzyl is nonplanar with the pyrimidine ring (Figure 13). The 2 phenylated azaindol system differs markedly from this orientation as shown in Figure 13.

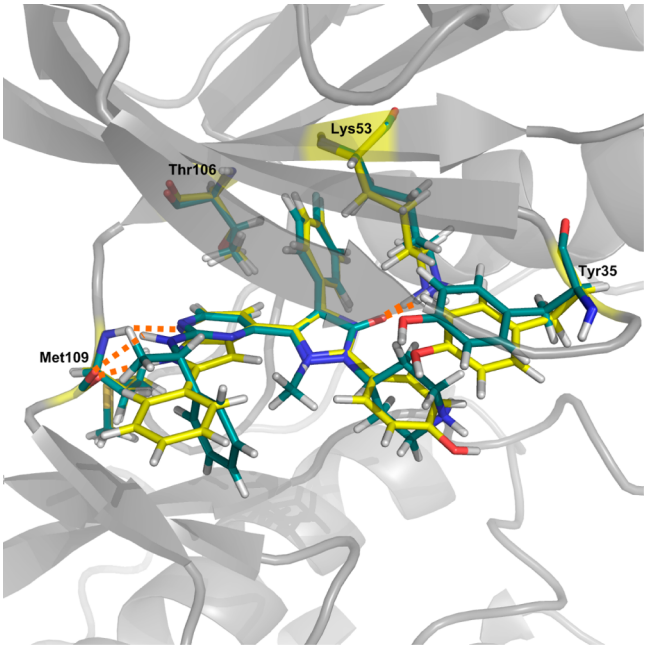

Figure 13. Overlay of the bound ligand of crystal structure 1YWR[25] and a 2-phenylated azaindole analogue of the herein synthesized inhibitors.

Nevertheless, our scaffold proved to be more efficient than the nonrigidized analogue (ML3403). In comparison to the previously determined IC_{50} values of the nonsubstituted analogue, only a 2-fold increase in the biological activity was observed.[9] In comparison to our unsubstituted analogue **14d**, we observed an 8-fold increase of the biological activity (compared by activity coefficients) (Tables 2 and 3).

dx.doi.org/10.1021/jm300852w | *J. Med. Chem.* 2012, 55, 8429−8439

The biological data clearly demonstrate the beneficial effect of the additional hydrogen bonding (**14c**) (Table 2), with a 1.4-fold increase in potency and an exceedingly strong hydrophobic effect for **14f** with a 5-fold increase (Table 3), compared to **14c**.

With the 2-phenylazaindole we observed a highly potent scaffold for interactions with the hinge region and with hydrophobic region II. With IC_{50} values as low as 16 nM, we further optimized our inhibitors by derivatization of the imidazole core (Figure 14) in stage V. The imidazole C-2

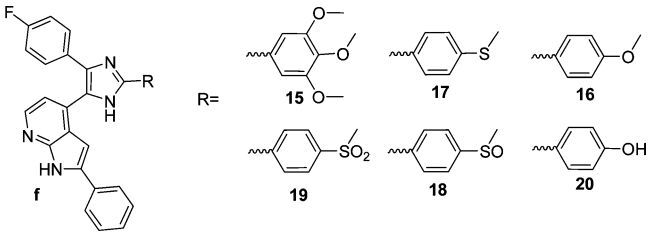

Figure 14. C-2 modifications of the imidazole core (derivatives **15f**–**20f**, stage V of optimization strategy).

position, bearing a phenyl substituent, has already been shown to be a less than ideal substituent.[3] Therefore, we investigated several aryl substituents at the imidazole C-2 position, combined with the most effective C-5 substituent, the phenylazaindole (Figure 14).

A trimethoxyphenyl substitution **15f** (Figure 14, Table 4) led to a decreased biological activity, while the methoxyphenyl

Table 4. Inhibition of p38 MAPK

compd	IC_{50} [μM][a]	gradient factor, IC_{50}(SB203580)/IC_{50}(compd)
17f	0.039 ± 0.0081	0.97
18f	0.008 ± 0.0003	4.75
19f	0.011 ± 0.0003	3.46
20f	0.003 ± 0.003	19.67
15f	0.290 ± 0.0453	0.12
16f	0.070 ± 0.0079	0.67

[a]Mean ± SEM of three experiments. Compounds tested according to Laufer et al.[24]

derivative **16f** displayed a better but still lower activity profile (Figure 14, Table 4). A meta substitution on the aryl derivative was poorly tolerated; therefore, we focused on the para-substituted aryl derivatizations in the following investigations. The *p*-methylsulfanyl derivative **17f** (Figure 14, Table 4) should serve as a direct analogue of the methoxy derivative **16f** (Figure 14, Table 4), with the effect of lower basicity of the heteroatom. An improved biological activity compared to the oxygen analogue was observed, but with respect to the reference compound **14f** (Figure 10, Table 3), the potency was clearly decreased. The common basis of these modifications is the lipophilic character of the performed derivatizations; therefore, the corresponding substitution patterns of the phenyl moiety were rendered more polar, in analogy to SB203580 and SB202190.[2] The methylsulfanyl was oxidized to the corresponding sulfoxide **18f** (Figure 14, Table 4), the structural analogue of SB203580, and a further oxidation yielded the corresponding sulfone **19f** (Figure 14, Table 4). Both inhibitors were superior to **14f** and SB203580 (Figure 14, Table 4), whereby the sulfoxide (racemic) proved to be the more potent derivative with a gradient factor of 4.75.

A dramatic increase in potency could be observed by the structural reduction of the *p*-methoxy moiety to the more polar *p*-hydroxy derivative **20f** (Figure 14, Table 4), the structural analogue of SB202190, with a nearly 20-fold increased potency, compared to the lead compound SB203580, and a 66-fold increased potency compared to our incipient reference compound **14d** (Figure 10, Table 2).

The accomplished docking studies of **20f** (Figure 15) gave similar results to that of **14f** (Figure 12). The role of the *p*-

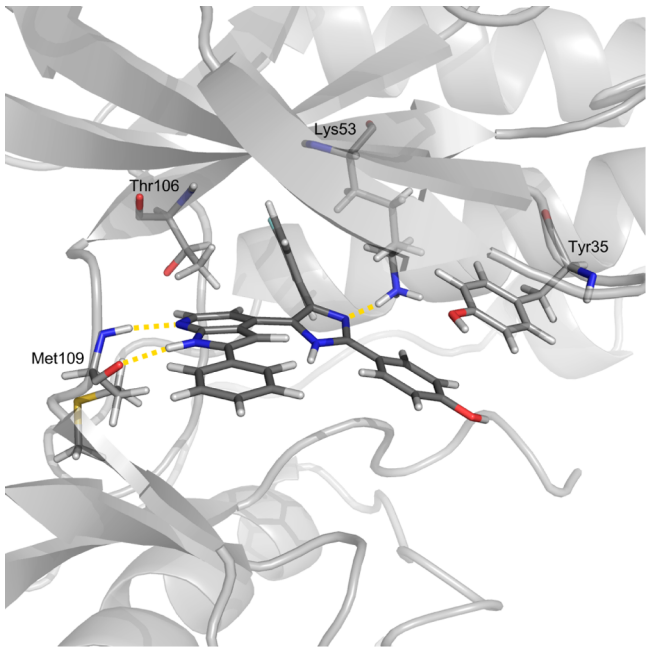

Figure 15. Docking results for **20f** in the p38 MAP kinase X-ray structure 1YWR[25] from the PDB database.

hydroxy group could not be elucidated by docking experiments. A possible explanation could be a participation of bridged water interactions, which might lead to an enhanced binding to the receptor.

For drug candidates interfering with protein kinases, their range of specifity within the kinome is a key question, and a robust evaluation of potency and selectivity is an essential part of drug discovery. Rigidization is a promising strategy in modern medicinal chemistry. Its objective is to synthetically fix a flexible ligand scaffold into a biologically relevant conformation with the overall intention to improve potency and selectivity of the corresponding ligands.[11] The herein evaluated inhibitors match this concept, and the selectivity of the most potent inhibitor **20f** was investigated for its selectivity toward other kinases. The corresponding analogue of **20f** is the well-known and already mentioned inhibitor SB202190, which is superior to SB203580 in regard to both potency and selectivity as shown by Fabian et al.[26] SB202190 was investigated in a panel of 119 kinases, and the compound showed significant inhibition of 14 kinases within this panel. Relevant inhibition was observed on kinases CSNK1E, EGFR, FRK, GAK, JNK1, JNK2, JNK3, p38α, p38β, p38γ, PTK6, RIPK2, STK36, and TNIK. In the same panel, compound **20f** showed an improved selectivity profile. Significant inhibition was observed toward the kinases GAK, CSNK1E, EGFR, p38α, p38β, RIPK2, SRC, STK36, and TNIK.

dx.doi.org/10.1021/jm300852w | J. Med. Chem. 2012, 55, 8429–8439

Table 5. Relevant Inhibition of 20f in a Panel of 119 Kinases

gene symbol (locus link)	gene symbol	kinase activity [%] at 1000 nM
CSNK1E	CSNK1E	17
EGFR	EGFR	2.8
GAK	GAK	7.7
MAPK14	p38α	8.9
MAPK11	p38β	2.5
RIPK2	RIPK2	3.2
SRC	SRC	28
STK36	STK36	4.8
KIAA0551	TNIK	17

Compared to SB202190, **20f** showed an improved selectivity profile in a panel of 119 kinases with a significant inhibition of 9 kinases whereas SB202190 showed significant inhibition of 14 kinases. The selectivity of compound **20f** was shown to be markedly improved within two kinase families the MAP kinase family and the tyrosin kinase family. Within the MAP kinases, compound **20f** showed only significant inhibition of p38α and p38β, whereas SB202190 shows inhibition of JNK1, JNK2, JNK3, p38α, p38β, and p38γ. Within the tyrosin kinase family, **20f** showed a completely different selectivity profile, inhibiting the SRC kinase, and SB202190 inhibited the FRK and PTK6 kinases.

A complete list of inhibition data for all 119 kinases is included in the Supporting Information.

CONCLUSION

Despite the extensive research of the class of pyridinylimidazoles as p38 MAPK inhibitors, no known investigation has focused on the concept of rigidization/aromatization. With the present inhibitor design, a fundamental structural change was successfully accomplished, leading to highly active inhibitors with IC_{50} values as low as 3 nM and a markedly improved selectivity profile. This study has given a platform to further investigate the pharmacological aspects of these promising modifications, based on a highly flexible and efficient synthetic procedure to provide further complex C-5 variations of the imidazole core.

EXPERIMENTAL SECTION

Molecular Modeling. All modeling was performed on an Ubuntu 10.04 LTS system. For visualization and building the structures, Maestro from Schrödinger (Maestro, version 9.1, Schrödinger, LLC, New York, NY, 2010) was used. The illustrations of modeling were generated by PyMol (version 0.99rc6). The docking studies were performed using the Induced Fit Docking protocol from Schrödinger (Schrödinger Suite 2010 Induced Fit Docking protocol; Glide, version 5.6, Schrödinger, LLC, New York, NY, 2010; Prime, version 2.2, Schrödinger, LLC, New York, NY, 2010). The PDB codes and references for the used X-ray structures are mentioned in the caption of the figures. In all docking studies mentioned here, the SP precision was used. The presented docking results were ranked highest.

The best docking pose of the corresponding ligand was minimized with MacroModel (MacroModel, version 9.8, Schrödinger, LLC, New York, NY, 2010) using the default settings (force field, OPLS 2005; solvent, water) and frozen atoms as constraints. After the minimization the hydrogen bond energy calculation was done using the Jaguar batch script hydrogen_bond.py (Jaguar, version 7.7, Schrödinger, LLC, New York, NY, 2010) which is integrated in the Schrödinger software suite. During this calculation there was no optimization for any structure and the fast mode was chosen. In the fast mode LMP2 (local Møller–Plesset perturbation theory) calculations are omitted and just DFT (density functional theory) energies were used.

Methods and Materials. All commercially available reagents and solvents were used without further purification. NMR data were obtained on a Bruker Spectrospin AC 200 instrument at ambient temperature. High-resolution spectral mass data were obtained on a Thermo Finnigan TSQ70 instrument. Melting points were measured on a Buechi melting point B-545 instrument. IR spectra were obtained by a Perkin-Elmer Spectrum One (ATR) instrument. LC–mass spectrometry (MS) spectra were recorded by a Finnigan TSQ Quantum triple quadrupole mass spectrometer (Finnigan MAT). GC–MS was done using a Hewlett-Packard HP 6890 series GC system (Hewlett-Packard HP 5973 mass selective detector). The purity of the final compounds was determined by HPLC on a Hewlett-Packard HP 1090 series II liquid chromatograph using a Betasil C8 column (150 mm × 4.6 mm i.d., dp = 5 μm, Thermo Fisher Scientific, Waltham, MA) at 230 and 254 nm, employing a gradient of 0.01 M KH_2PO_4 (pH 2.3) and methanol as the solvent system with a flow rate of 1.5 mL/min. All final compounds have a purity of >96% (see Supporting Information for details).

General Procedure of Stille Coupling. A premilled mixture (0.1 mol % Pd) of $Pd(OAc)_2$ and X-Phos ($^1/_3$) was stirred in dioxane for 30 min, and the yellow solution turned to a dark purple solution. The halogenated N-protected heterocycle and the stannylimidazole (2 equiv) were added to the reaction mixture and heated under microwave irradiation (300 W, 100 °C, 10–15 min) in a sealed tube under nitrogen atmosphere and instant cooling. After quenching with KF (40% in water) and extracting with EtOAc, the crude product was purified by flash chromatography.

General Procedure for MOM Deprotection. The MOM protected compound was dissolved in a mixture of aqueous HCl/MeOH (4/1). The reaction mixture was heated under reflux until complete conversion to the product (monitoring by HPLC). After removal of the solvent, the crude product was neutralized with $NaHCO_3$ and extracted with ethyl acetate and subjected to flash chromatography.

General Procedure for Detosylation. The educt was dissolved in MeOH. After addition of Cs_2CO_3, the mixture was heated to reflux until complete conversion to the product. The solvent was removed, and water was added to the crude product. After extraction with ethyl acetate, the crude product was subjected to flash chromatography.

6-[4-(4-Fluorophenyl)-1-(methoxymethyl)-2-phenyl-1*H*-imidazol-5-yl]-9*H*-purine (15a). Yield, 46%; $C_{22}H_{17}FN_6O$ (M_r = 400.41); ^{1}H NMR (200 MHz, acetone-d_6) δ ppm 2.89 (s, 3 H, $MOMCH_3$), 5.59 (s, 2 H, $MOMCH_2$), 6.92 (m, 2 H, *m*-4FPhH), 7.53 (m, 6 H, *o*-/*m*-/*p*-PhH, Pyr.6-H, PurH), 7.90 (m, 2 H, *o*-4FPhH), 8.38 (s, 1 H, Pur.2-H), 9.03 (m, 1 H, NH); ^{13}C NMR (50.33 MHz, acetone-d_6) δ ppm 555.0, 75.4, 114.5 (d, J_{C-F} = 21.5 Hz), 123.7, 125.6, 128.3, 128.5, 128.6, 128.7, 129.1 (d, J_{C-F} =8.1 Hz), 129.2, 130.5, 131.0 (d, J_{C-F} =3.1 Hz), 131.6, 131.7, 131.8, 131.8, 141.0, 145.3, 150.2, 161.9 (d, J_{C-F} = 244.0 Hz); HRMS (ESI) calcd for $C_{22}H_{17}FN_6O$ $[M + H]^+$ 401.152 06, found 401.151 701 (error 0.90 ppm).

4-[4-(4-Fluorophenyl)-1-(methoxymethyl)-2-phenyl-1*H*-imidazol-5-yl]-7*H*-pyrrolo[2,3-*d*]pyrimidine (15b). Yield, 42%; $C_{23}H_{18}FN_5O$ (M_r = 399,42); ^{1}H NMR (200 MHz, methanol-d_4) δ ppm 2.79 (s, 3 H, $MOMCH_3$), 5.46 (s, 2 H, $MOMCH_2$), 5.89 (d, J = 3.41 Hz, 1 H, Pyr.6-H), 6.87 (m, 2 H, *m*-4FPhH), 7.29 (m, 3 H, *o*-4FPhH, Pyr.5H), 7.49 (m, 3 H, *m*-/*p*-PhH), 7.75 (m, 2 H, *o*-PhH), 8.83 (s, 1 H, NH); ^{13}C NMR (50.33 MHz, methanol-d_4) δ ppm 54.7, 75.4, 100.1, 114.7 (d, J_{C-F} = 21.9 Hz), 117.7, 125.1, 127.4, 128.4, 129.3, 129.4, 129.7, 140.6, 148.6, 150.5, 151.2, 152.0, 162.3 (d, J_{C-F} = 246.2 Hz); HRMS (ESI) calcd for $C_{23}H_{18}FN_5O$ $[M + H]^+$ 400.156 81, found 400.156 528 (error 0.71 ppm).

4-[4-(4-Fluorophenyl)-1-(methoxymethyl)-2-phenyl-1*H*-imidazol-5-yl]-1*H*-pyrrolo[2,3-*b*]pyridine (15c). Yield, 96%; $C_{24}H_{19}FN_4O$ (M_r = 398.43); ^{1}H NMR (200 MHz, $CDCl_3$) δ ppm 3.05 (m, 3 H, $MOMCH_3$), 5.10 (m, 2 H, $MOMCH_2$), 6.11 (m, 1 H, Aza2-H), 6.91 (m, 2 H, *m*-4FPhH), 7.36 (m, 5 H, *m*-/*p*-PhH, Aza3-H), 7.58 (m, 3 H, Aza5-H, *o*-4FPhH), 7.89 (m, 2 H, *o*-PhH), 8.35 (m, 1 H, Aza6-H); ^{13}C NMR (50.33 MHz, methanol-d_4) δ ppm 54.5, 75.0,

dx.doi.org/10.1021/jm300852w | J. Med. Chem. 2012, 55, 8429–8439

99.6, 114.5 (d, J_{C-F} = 21.8 Hz), 117.1, 120.3, 120.3, 1265, 128.4, 126.7 (d, J_{C-F} = 8.1 Hz), 129.0, 129.4, 129.5, 128.8 (d, J_{C-F} = 3.1 Hz), 130.3, 137.9, 142.0, 148.3, 162.0 (d, J_{C-F} = 245.8 Hz); HRMS (ESI) calcd for $C_{24}H_{19}FN_4O$ $[M + H]^+$ 399.161 57, found 399.161 961 (error 0.98 ppm).

6-[4-(4-Fluorophenyl)-2-phenyl-1*H*-imidazol-5-yl]-9*H*-purine (14a). Yield, 57%; $C_{20}H_{13}FN_6$ (M_r = 356.36); ^{1}H NMR (200 MHz, methanol-d_4/DMSO-d_6) δ ppm 7.14 (m, 2 H, *m*-4FPhH), 7.42 (m, 3 H, *m*-/*p*-4FPhH), 7.82 (m, 2 H, *o*-4FPhH), 8.17 (d, J = 6.82 Hz, 2 H, *o*-PhH), 8.47 (s, 1 H, Pur.8-H), 8.66 (s, 1 H, Pur.2-H); ^{13}C NMR (100.66 MHz, DMSO-d_6) δ ppm 114.6 (d, J_{C-F} = 22.0 Hz), 125.9, 128.7, 129.0, 129.5, 132.0, 145.6, 146.8, 147.3, 151.5, 162.0 (d, J_{C-F} = 245.9 Hz); HRMS (ESI) calcd for $C_{20}H_{13}FN_6$ $[M + H]^+$ 357.1285, found 357.125 623 (error 0.64 ppm).

4-[4-(4-Fluorophenyl)-2-phenyl-1*H*-imidazol-5-yl]-7*H*-pyrrolo[2,3-*d*]pyrimidine (14b). Yield, 85%; $C_{21}H_{14}FN_5$ (M_r = 355.37); ^{1}H NMR (200 MHz, DMSO-d_6) δ ppm 5.86 (s, 1 H, Pyr.5-H), 7.32 (m, 2 H, *m*-4FPhH), 7.63 (m, 7 H, *m*-/*p*-PhH, *o*-4FPhH, Pyr.6-H), 8.27 (m, 2 H, *o*-PhH), 8.99 (m, 1 H, Pyr.2-H), 13.17 (m, 1 H, NH); ^{13}C NMR (50.33 MHz, DMSO-d_6) δ ppm 103.1, 113.6, 116.1 (d, J_{C-F} = 21.5 Hz), 125.6, 126.7, 127.8, 128.4 (d, J_{C-F} = 4.2 Hz), 129.3, 129.3, 130.5 (d, J_{C-F} = 8.8 Hz), 132.0, 132.1, 136.4, 136.5, 145.6, 146.5, 148.0, 152.5, 168.2 (d, J_{C-F} = 273.8 Hz); HRMS (ESI) calcd for $C_{21}H_{14}FN_5$ $[M + H]^+$ 356.130 60, found 356.130 892 (error 0.82 ppm).

4-[4-(4-Fluorophenyl)-2-phenyl-1*H*-imidazol-5-yl]-1*H*-pyrrolo[2,3-*b*]pyridine (14c). Yield, 82%; $C_{22}H_{15}FN_4$ (M_r = 354.38); ^{1}H NMR (200 MHz, methanol-d_4) δ ppm 6.08 (m, 1 H, Aza2-H), 6.94 (m, 2 H, *o*-4FPhH), 7.11 (d, J = 5.05 Hz, 1 H, Aza5-H), 7.18 (d, J = 3.54 Hz, 1 H, Aza3-H), 7.38 (m, 6 H, *m*-/*p*-PhH, *o*-4FPhH), 7.94 (m, 2 H, *o*-PhH), 8.10 (d, J = 5.31 Hz, 1 H, Aza6-H); ^{13}C NMR (50.33 MHz, methanol-d_4) δ ppm 100.5, 114.8 (d, J_{C-F} = 21.5 Hz), 118.5, 125.4, 125.4, 125.5, 128.5, 128.7, 129.6 (d, J_{C-F} = 6.1 Hz), 129.7, 141.6, 147.6, 148.3, 162.2 (d, J_{C-F} = 246.0 Hz); HRMS (ESI) calcd for $C_{22}H_{15}FN_4$ $[M + H]^+$ 355.135 35, found 355.135 511 (error 0.45 ppm).

4-[4-(4-Fluorophenyl)-2-phenyl-1*H*-imidazol-5-yl]-9*H*-pyrido[2,3-*b*]indole (14e). Yield, 69%; $C_{26}H_{17}FN_4$ (M_r = 404.44); ^{1}H NMR (200 MHz, methanol-d_4) δ ppm 6.86 (m, 3 H, *m*-4FPhH), 7.08 (d, J = 4.55 Hz, 1 H, Carb.H), 7.40 (m, 8 H, *m*-/*p*-PhH, *o*-4FPhH), 7.95 (m, 2 H, *o*-PhH), 8.27 (m, 1 H, Carb.2-H); ^{13}C NMR (50.33 MHz, methanol-d_4) δ ppm 112.3, 116.5 (d, J_{C-F} = 22.2 Hz), 117.9, 121.1, 121.3, 123.7, 127.3, 128.4, 129.7, 130.3, 130.5 (d, J_{C-F} = 8.4 Hz), 131.1, 134.4, 136.2, 140.8, 145.9, 151.0 (d, J_{C-F} = 230.4 Hz); HRMS (ESI) calcd for $C_{26}H_{17}FN_4$ $[M + H]^+$ 405.151 00, found 405.150 678 (error 0.80 ppm).

2-Benzyl-4-[4-(4-fluorophenyl)-2-phenyl-1*H*-imidazol-5-yl]-1*H*-pyrrolo[2,3-*b*]pyridine (14g). Yield, 65%; $C_{29}H_{21}FN_4$ (M_r = 444.5); ^{1}H NMR (400 MHz, acetone-d_6/methanol-d_4) δ ppm 3.93 (s, 2 H, $BzCH_2$), 6.96 (m, 2 H, Aza3-H/Aza5-H), 7.06 (m, 2 H, *o*-BzH), 7.18 (m, 5 H, *m*-/*p*-BzH, *m*-4FPhH), 7.35 (m, 3 H, *m*-/*p*-ArH), 7.44 (m, 2 H, *o*-4FPhH), 7.98 (d, J = 7.33 Hz, 2 H, *o*-PhH), 8.09 (m, 1 H,Aza6-H). ^{13}C could not be detected because of insolubility of the compound. HRMS (ESI) calcd for $C_{29}H_{21}FN_4$ $[M + H]^+$ 445.182 30, found 445.182 466 (error 0.37 ppm).

4-[4-(4-Fluorophenyl)-2-phenyl-1*H*-imidazol-5-yl]-2-phenyl-1*H*-pyrrolo[2,3-*b*]pyridine (14f). Yield, 90%; $C_{28}H_{19}FN_4$ (M_r = 430.48); ^{1}H NMR (200 MHz, $CDCl_3$) δ ppm 6.80 (s, 1 H, NH), 7.10 (m, 2 H, *o*-4FPhH), 7.21 (d, J = 4.80 Hz, 1 H, Aza3-H), 7.42 (brm, 7 H, PhH, Aza5-H), 7.63 (m, 2 H, *m*-4FPhH), 7.86 (d, J = 7.20 Hz, 2 H, *o*-PhH), 8.14 (d, J = 8.59 Hz, 1 H, Aza6-H), 8.22 (m, 2 H, *o*-PhH), 11.85 (m, 1 H, NH); ^{13}C NMR (50.33 MHz, acetone-d_6) 98.5, 114.97 (d, J_{C-F} = 21.3 Hz), 119.3, 125.4, 125.8, 126.0, 127.1, 128.0, 128.5 (d, J_{C-F} = 8.5 Hz), 128.9, 129.8, 130.5, 132.0, 138.5, 139.5, 142.6, 146.4, 146.7, 150.8, 162 (d, J_{C-F} = 244.1 Hz); HRMS (ESI) calcd for $C_{28}H_{19}FN_4$ $[M + H]^+$ 431.166 65, found 431.166 381 (error 0.62 ppm).

2-Cyclohexyl-4-[4-(4-fluorophenyl)-2-phenyl-1*H*-imidazol-5-yl]-1*H*-pyrrolo[2,3-*b*]pyridine (14h). Yield, 85%; $C_{28}H_{25}FN_4$ (M_r = 436.52); ^{1}H NMR (200 MHz, $CDCl_3$) δ ppm 1.29 (m, 6 H, ChH), 1.84 (m, 4 H, ChH), 2.69 (m, 1 H, ipso-ChH), 6.04 (m, 1 H, Aza3-H), 6.95 (m, 2 H, *m*-4FPhH), 7.13 (d, J = 5.43 Hz, 1 H, Aza5-H), 7.46 (m, 6 H, *m*-/*p*-PhH, *o*-4FPhH, NH), 7.95 (m, 1 H, Aza6-H), 8.04 (m, 2 H, *o*-PhH), 10.68 (s, 1 H, NH); ^{13}C NMR (50.33 MHz, DMSO-d_6) δ ppm 25.6, 31.9, 33.9, 36.5, 45.2, 95.6, 114.7, 115.1 [(d, J_{C-F} = 21.47 Hz), 118.0, 125.5, 128.6 (d, J_{C-F} = 8.06 Hz), 128.7, 129.7, 129.8 (br), 129.9, 140.7, 146.1, 149.0, 161.4 (d, J_{C-F} = 245.0 Hz); HRMS (ESI) calcd for $C_{28}H_{25}FN_4$ $[M + H]^+$ 437.213 60, found 437.213 892 (error 0.67 ppm).

4-[4-(4-Fluorophenyl)-2-(3,4,5-trimethoxyphenyl)-1*H*-imidazol-5-yl]-2-phenyl-1*H*-pyrrolo[2,3-*b*]pyridine (15f). Yield, 84%; $C_{31}H_{25}FN_4O_3$ (M_r = 520.55); ^{1}H NMR (200 MHz, DMSO-d_6) δ ppm 3.71 (s, 3 H, *p*-OCH_3), 3.87 (s, 6 H, *m*-OCH_3), 6.60 (m, 1 H, Aza3-H), 7.12 (m, 2 H, *m*-4FPhH), 7.41 (m, 8 H, Aza5-H, *o*-ArH, *o*-4FPhH, *m*-/*p*-4FPhH), 7.76 (m, 2 H, *o*-PhH), 8.23 (m, 1 H, Aza6-H), 12.18 (m, 1 H, NH), 12.88 (m, 1 H, NH); ^{13}C NMR (50.33 MHz, DMSO-d_6) δ ppm 56.0, 60.1, 97.8, 102.8, 115.3 (d, J_{C-F} = 20.7 Hz), 118.7, 125.2, 125.6, 128.0, 128.9, 129.7 (d, J_{C-F} = 3.1 Hz), 131.5, 137.9, 142.8, 146.2, 150.4, 153.2, 161.4 (d, J_{C-F} = 245.8 Hz); HRMS (ESI) calcd for $C_{31}H_{25}FN_4O_3$ $[M + H]^+$ 521.198 35, found 521.198 712 (error 0.70 ppm).

4-[4-(4-Fluorophenyl)-2-(4-methoxyphenyl)-1*H*-imidazol-5-yl]-2-phenyl-1*H*-pyrrolo[2,3-*b*]pyridine (16f). Yield, 75%; $C_{29}H_{21}FN_4O$ (M_r = 460.5); ^{1}H NMR (200 MHz, DMSO-d_6/methanol-d_4) δ ppm 3.90 (s, 3 H, OCH_3), 6.49 (brm, 1 H, Aza-3-H), 7.10 (m, 4 H, *m*-4FPhH, *m*-ArH), 7.23 (d, J = 5.05 Hz, 1 H, Aza5-H), 7.45 (m, 5 H, *m*-/*p*-PhH, *o*-4FPhH), 7.72 (m, 2 H, *o*-PhH), 8.05 (d, J = 8.97 Hz, 2 H, *o*-ArH), 8.23 (brs, 1 H, Aza6-H); HRMS (ESI) calcd for $C_{29}H_{21}FN_4O$ $[M + H]^+$ 461.177 22, found 461.177 353 (error 0.29 ppm).

4-{4-(4-Fluorophenyl)-2-[4-(methylthio)phenyl]-1*H*-imidazol-5-yl}-2-phenyl-1*H*-pyrrolo[2,3-*b*]pyridine (17f). Yield, 69%; $C_{29}H_{21}FN_4S$ (M_r = 476.57); ^{1}H NMR (200 MHz, methanol-d_4/DMSO-d_6) δ ppm 2.45 (s, 3 H, SCH_3), 6.46 (s, 1 H, Aza3-H), 7.05 (m, 3 H, *m*-4FPhH, Aza5-H), 7.29 (m, 5 H, *m*-$PhSCH_3$, *m*-/*p*-PhH), 7.45 (m, 2 H, *o*-4FPhH), 7.64 (d, J = 7.07 Hz, 2 H, *m*-PhH), 7.97 (d, J = 8.34 Hz, 2 H, *o*-$PhSCH_3$), 8.12 (d, J = 5.05 Hz, 1 H, Aza6-H); ^{13}C NMR (50.33 MHz, methanol-d_4/DMSO-d_6) δ ppm 99.3, 116.5 (d, J_{C-F} =21.4 Hz), 116.9, 120.6, 121.1, 126.7, 127.4 (d, J_{C-F} = 8.4 Hz), 127.9, 129.4, 130.2, 131.4 (d, J_{C-F} = 4.9 Hz), 133.1, 139.9, 141.2, 143.9, 147.0, 148.2, 151.7, 163.1 (d, J_{C-F} = 245.8 Hz); HRMS (ESI) calcd for $C_{29}H_{21}FN_4S$ $[M + H]^+$ 477.154 37, found 477.154 424 (error 0.11 ppm).

4-[4-(4-Fluorophenyl)-5-(2-phenyl-1*H*-pyrrolo[2,3-*b*]pyridin-4-yl)-1*H*-imidazol-2-yl]phenol (20f). Yield, 88%; $C_{28}H_{19}FN_4O$ (M_r = 446.48); ^{1}H NMR (200 MHz, methanol-d_4/DMSO-d_6) δ ppm 6.74 (s, 1 H, Aza3-H), 7.15 (d, J = 8.59 Hz, 2 H, *m*-PhOH), 7.36 (m, 2 H, *m*-4FPhH), 7.46 (d, J = 5.05 Hz, 1 H, Aza5-H), 7.68 (m, 5 H, *o*-4FPhH, *m*-PhH, *p*-PhH), 7.96 (d, J = 7.07 Hz, 2 H, *m*-PhH), 8.17 (d, J = 8.84 Hz, 2 H, *o*-PhOH), 8.46 (d, J = 5.31 Hz, 1 H, Aza6-H); ^{13}C NMR (50.33 MHz, methanol-d_4/DMSO-d_6) δ ppm 99.3, 116.4 (d, J_{C-F} = 21.9 Hz), 116.9, 117.2, 120.6, 122.0, 126.6, 128.7, 129.3, 130.2, 131.3 (d, J_{C-F} = 8.1 Hz), 133.1, 139.8, 143.8, 149.5, 151.6, 163.4 (d, J_{C-F} = 245.8 Hz); HRMS (ESI) calcd for $C_{28}H_{19}FN_4O$ $[M + H]^+$ 447.161 57, found 447.161 709 (error 0.31 ppm).

4-{4-(4-Fluorophenyl)-2-[4-(methylsulfinyl)phenyl]-1*H*-imidazol-5-yl}-2-phenyl-1*H*-pyrrolo[2,3-*b*]pyridine (18f). Yield, 57%; $C_{29}H_{21}FN_4OS$ (M_r = 492.57); ^{1}H NMR (200 MHz, methanol-d_4) δ ppm 2.84 (s, 3 H, $SOCH_3$), 6.45 (s, 1 H, Aza3H), 7.07 (m, 2 H, *m*-4FPhH), 7.21 (d, J = 5.05 Hz, 1 H, Aza 5-H), 7.40 (m, 5 H, *m*-/*p*-PhH, *o*-4FPhH), 7.65 (m, 2 H, *o*-PhH), 7.83 (d, J = 8.72 Hz, 2 H, *m*-ArH), 8.17 (m, 1 H, Aza6-H), 8.26 (d, J = 8.72 Hz, 2 H, *o*-ArH); ^{13}C NMR (50.33 MHz, methanol-d_4/DMSO-d_6) δ ppm 43.5, 99.1,110.8, 116.5 (d, J_{C-F} = 21.9 Hz), 119.6, 125.6, 126.6, 127.9, 129.3, 123.0, 131.4 (d, J_{C-F} = 8.4 Hz), 133.1, 134.1, 140.6, 142.4, 143.3, 146.4, 147.6, 151.2, 164.0 (d, J_{C-F} = 246.9 Hz); HRMS (ESI) calcd for $C_{29}H_{21}FN_4OS$ $[M + H]^+$ 493.149 29, found 493.149 568 (error 0.58 ppm).

4-{4-(4-Fluorophenyl)-2-[4-(methylsulfonyl)phenyl]-1*H*-imidazol-5-yl}-2-phenyl-1*H*-pyrrolo[2,3-*b*]pyridine (19f). Yield,

50%; $C_{29}H_{21}FN_4O_2S$ (M_r = 508.57); ^{1}H NMR (400 MHz, methanol-d_4) δ ppm 3.04 (s, 3 H, SO_2CH_3), 6.54 (s, 1 H, aza3-H), 6.96 (m, 2 H, *m*-4FPhH), 7.12 (m, 1 H), 7.23 (d, J = 7.33 Hz, 1 H, Aza5-H), 7.31 (m, 2 H, *o*-4FPhH), 7.41 (m, 2 H, *o*-PhH), 7.56 (m, 3 H, *m*-/*p*-PhH), 7.94 (d, J = 8.34 Hz, 1 H, *o*-$PhSO_2H$), 8.05 (m, 1 H, aza6-H), 8.22 (d, J = 8.34 Hz, 2 H, *m*-$PhSO_2H$); ^{13}C NMR (200 MHz, DMSO-d_6) δ ppm 43.2, 96.2, 115.3 (d, J_{C-F} = 21.5 Hz), 117.9, 120.6, 125.6, 127.2, 128.2, 128.3, 128.5, 128.9, 129.4 (d, J_{C-F} = 3.1 Hz), 129.8, 131.0, 136.8, 140.0, 143.1, 150.1, 161.4 (d, J_{C-F} = 244.6 Hz); HRMS (ESI) calcd for $C_{29}H_{21}FN_4O_2S$ $[M + H]^+$ 509.144 20, found 509.144 424 (error 0.44 ppm).

■ ASSOCIATED CONTENT

Supporting Information

Experimental procedures, analytical data, detailed selectivity data, and the molecular modeling. This material is available free of charge via the Internet at http://pubs.acs.org.

■ AUTHOR INFORMATION

Corresponding Author

*Phone: +49-70712978788. Fax: +49-7071295037. E-mail: stefan.laufer@uni-tuebingen.de.

Notes

The authors declare no competing financial interest.

■ ACKNOWLEDGMENTS

The authors thank the Federal Ministry of Education and Research, Germany, Merckle GmbH, Ulm, Germany, the BASF Group, especially Dr. Martin Fiene, and the Fonds der Chemischen Industrie, Germany, for their generous support of this work.

■ REFERENCES

(1) Lee, J. C.; Griswold, D. E.; Votta, B.; Hanna, N. Inhibition of monocyte IL-1 production by the anti-inflammatory compound, SK & F 86002. *Int. J. Immunopharmacol.* **1988**, *10*, 835−843.

(2) Adams, J. L.; Gallagher, T. F.; Lee, J. Imidazole Derivatives and Their Use as Cytokine Inhibitors. U.S. Patent WO93114081, 1993.

(3) Peifer, C.; Kinkel, K.; Abadleh, M.; Schollmeyer, D.; Laufer, S. From five- to six-membered rings: 3,4-diarylquinolinone as lead for novel p38MAP kinase inhibitors. *J. Med. Chem.* **2007**, *50*, 1213−1221.

(4) Gallagher, T. F.; Seibel, G. L.; Kassis, S.; Laydon, J. T.; Blumenthal, M. J.; Lee, J. C.; Lee, D.; Boehm, J. C.; Fier-Thompson, S. M.; Abt, J. W.; Soreson, M. E.; Smietana, J. M.; Hall, R. F.; Garigipati, R. S.; Bender, P. E.; Erhard, K. F.; Krog, A. J.; Hofmann, G. A.; Sheldrake, P. L.; McDonnell, P. C.; Kumar, S.; Young, P. R.; Adams, J. L. Regulation of stress-induced cytokine production by pyridinylimidazoles; inhibition of CSBP kinase. *Bioorg. Med. Chem.* **1997**, *5*, 49−64.

(5) Wang, Z.; Canagarajah, B. J.; Boehm, J. C.; Kassisa, S.; Cobb, M. H.; Young, P. R.; Abdel-Meguid, S.; Adams, J. L.; Goldsmith, E. J. Structural basis of inhibitor selectivity in MAP kinases. *Structure* **1998**, *6*, 1117−11128.

(6) Selig, R.; Schattel, V.; Goettert, M.; Schollmeyer, D.; Albrecht, W.; Laufer, S. Conformational effects on potency of thioimidazoles and dihydrothiazolines. *MedChemComm* **2011**, *2*, 261−269.

(7) Margutti, S.; Laufer, S. A. Are MAP kinases drug targets? Yes, but difficult ones. *ChemMedChem* **2007**, *2*, 1116−1140.

(8) Boehm, J. C.; Smietana, J. M.; Sorenson, M. E.; Garigipati, R. S.; Gallagher, T. F.; Sheldrake, P. L.; Bradbeer, J.; Badger, A. M.; Laydon, J. T. 1-Substituted 4-aryl-5-pyridinylimidazoles: a new class of cytokine suppressive drugs with low 5-lipoxygenase and cyclooxygenase inhibitory potency. *J. Med. Chem.* **1996**, *39*, 3929−3937.

(9) Wagner, G.; Laufer, S. Small molecular anti-cytokine agents. *Med. Res. Rev.* **2006**, *26*, 1−62.

(10) Laufer, S. A.; Wagner, G. K.; Kotschenreuther, D. A.; Albrecht, W. Novel substituted pyridinyl imidazoles as potent anticytokine agents with low activity against hepatic cytochrome P450 enzymes. *J. Med. Chem.* **2003**, *46*, 3230−3244.

(11) *The Practice of Medicinal Chemistry*; Wermuth, C. G., Ed.; Elsevier: Amsterdam, The Netherlands, 2008.

(12) Velazquez-Campoy, A.; Luque, I.; Freire, E. The application of thermodynamic methods in drug design. *Thermochim. Acta* **2001**, *380*, 217−227.

(13) Veber, D. F.; Johnson, S. R.; Cheng, H. Y.; Smith, B. R.; Ward, K. W.; Kopple, K. D. Molecular properties that influence the oral bioavailability of drug candidates. *J. Med. Chem.* **2002**, *45*, 2615−2623.

(14) Selig, R.; Schollmeyer, D.; Albrecht, W.; Laufer, S. The application of Stille cross-coupling reactions with multiple nitrogen containing heterocycles. *Tetrahedron* **2011**, *67*, 9204−9213.

(15) Hartwig, J. F. Discovery and understanding of transition-metal-catalyzed aromatic substitution reactions. *Synlett* **2006**, 1283−1294.

(16) Robins, R. K.; Godefroi, E. F.; Taylor, E. C.; Lewis, L. R.; Jackson, A. Purine nucleosides. I. The synthesis of certain 6-substituted-9-(tetrahydro-2-pyranyl)purines as models of purine deoxynucleosides. *J. Am. Chem. Soc.* **1961**, *83*, 2574−2579.

(17) Mendiola, J.; Baeza, A.; varez-Builla, J.; Vaquero, J. J. Reaction of bromomethylazoles and tosylmethyl isocyanide. A novel heterocyclization method for the synthesis of the core of marine alkaloids variolins and related azolopyrimidines. *J. Org. Chem.* **2004**, *69*, 4974−4983.

(18) Liverton, N. J.; Butcher, J. W.; Claiborne, C. F.; Claremon, D. A.; Libby, B. E.; Nguyen, K. T.; Pitzenberger, S. M.; Selnick, H. G.; Smith, G. R.; Tebben, A.; Vacca, J. P.; Varga, S. L.; Agarwal, L.; Dancheck, K.; Forsyth, A. J.; Fletcher, D. S.; Frantz, B.; Hanlon, W. A.; Harper, C. F.; Hofsess, S. J.; Kostura, M.; Lin, J.; Luell, S.; O'Neill, E. A.; Orevillo, C. J.; Pang, M.; Parsons, J.; Rolando, A.; Sahly, Y.; Visco, D. M.; O'Keefe, S. J. Design and synthesis of potent, selective, and orally bioavailable tetrasubstituted imidazole inhibitors of p38 mitogen-activated protein kinase. *J. Med. Chem.* **1999**, *42*, 2180−2190.

(19) Ahlquist, M.; Fristrup, P.; Tanner, D.; Norrby, P. O. Theoretical evidence for low-ligated palladium(0): [Pd-L] as the active species in oxidative addition reactions. *Organometallics* **2006**, *25*, 2066−2073.

(20) Cox, P. J.; Majid, T. N.; Lai, J. Y. Q.; Morley, A. D.; Amendola, S.; Deprets, S. Preparation of Azaindoles as Protein Kinase Inhibitors. U.S. Patent WO2001047922, 2000.

(21) Maresh, J. J.; Giddings, L. A.; Friedrich, A.; Loris, E. A.; Panjikar, S.; Trout, B. L.; Stoeckigt, J.; Peters, B.; O'Connor, S. E. Strictosidine synthase: mechanism of a Pictet−Spengler catalyzing enzyme. *J. Am. Chem. Soc.* **2008**, *130*, 710−723.

(22) Bajwa, J. S.; Chen, G. P.; Prasad, K.; Repic, O.; Blacklock, T. J. Deprotection of N-tosylated indoles and related structures using cesium carbonate. *Tetrahedron Lett.* **2006**, *47*, 6425−6427.

(23) Sasaki, Y.; Kato, D.; Boger, D. L. Asymmetric total synthesis of vindorosine, vindoline, and key vinblastine analogues. *J. Am. Chem. Soc.* **2010**, *132*, 13533−13544.

(24) Laufer, S.; Thuma, S.; Peifer, C.; Greim, C.; Herweh, Y.; Albrecht, W.; Dehner, F. An immunosorbent, nonradioactive p38 MAP kinase assay comparable to standard radioactive liquid-phase assays. *Anal. Biochem.* **2005**, *344*, 135−137.

(25) Golebiowski, A.; Townes, J. A.; Laufersweiler, M. J.; Brugel, T. A.; Clark, M. P.; Clark, C. M.; Djung, J. F.; Laughlin, S. K.; Sabat, M. P.; Bookland, R. G.; VanRens, J. C.; De, B.; Hsieh, L. C.; Janusz, M. J.; Walter, R. L.; Webster, M. E.; Mekel, M. J. The development of monocyclic pyrazolone based cytokine synthesis inhibitors. *Bioorg. Med. Chem. Lett.* **2005**, *15*, 2285−2289.

(26) Fabian, M. A.; Biggs, W. H.; Treiber, D. K.; Atteridge, C. E.; Azimioara, M. D.; Benedetti, M. G.; Carter, T. A.; Ciceri, P.; Edeen, P. T.; Floyd, M.; Ford, J. M.; Galvin, M.; Gerlach, J. L.; Grotzfeld, R. M.; Herrgard, S.; Insko, D. E.; Insko, M. A.; Lai, A. G.; Lelias, J. M.; Mehta, S. A.; Milanov, Z. V.; Velasco, A. M.; Wodicka, L. M.; Patel, H. K.; Zarrinkar, P. P.; Lockhart, D. J. A small molecule-kinase interaction map for clinical kinase inhibitors. *Nat. Biotechnol.* **2005**, *23*, 329−336.